

Model^{11,12,13,14,15}. However, this is not unambiguous evidence of new physics. The contribution of intermediate $c\bar{c}$ loops, referred to as a ‘long-distance’ or ‘non-local’ effect, gives a contribution to the amplitudes that is identical to the C_9 Wilson coefficient. These $c\bar{c}$ loops are difficult to calculate and so a source of significant uncertainty in the theory predictions. In this analysis the experimental data has been used to try and estimate the size of these long-distance effects in $B^0 \rightarrow K^{*0}\mu^+\mu^-$ ^{16,17}.

2 Analysis

The decay $B^0 \rightarrow K^{*0}\mu^+\mu^-$ is completely described by three decay angles, $\Omega = (\cos\theta_\ell, \cos\theta_K, \phi)$, and the invariant mass squared of the two muons, q^2 . The differential decay rate is expressed as the sum of angular terms

$$\begin{aligned} \frac{d^4\Gamma_P}{dq^2d\Omega} = \frac{9}{32\pi} & [J_{1s}\sin^2\theta_K + J_{1c}\cos^2\theta_K + (J_{2s}\sin^2\theta_K + J_{2c}\cos^2\theta_K)\cos 2\theta_\ell \\ & + J_3\sin^2\theta_K\sin^2\theta_\ell\cos 2\phi + J_4\sin 2\theta_K\sin 2\theta_\ell\cos\phi + J_5\sin 2\theta_K\sin\theta_\ell\cos\phi \\ & + J_{6s}\sin^2\theta_K\cos\theta_\ell + J_7\sin 2\theta_K\sin\theta_\ell\sin\phi + J_8\sin 2\theta_K\sin 2\theta_\ell\sin\phi \\ & + J_9\sin^2\theta_K\sin^2\theta_\ell\sin 2\phi], \end{aligned}$$

where the J_i coefficients are dependent on q^2 . The angular coefficients are combinations of the q^2 -dependent amplitudes $\mathcal{A}_\lambda^{L,R}$, where $\lambda = \parallel, \perp, 0$ labels the polarisation state of the K^{*0} . These amplitudes themselves are functions of the Wilson coefficients that describe the short-distance physics of the $b \rightarrow s\mu\mu$ transition. They also depend on the local form factors, \mathcal{F}_λ that describe the hadronic physics of $B \rightarrow K^{*0}$ and non-local form factors, \mathcal{H}_λ , that parametrise the effect of the $c\bar{c}$ loops. For example

$$\mathcal{A}_\parallel \sim \left\{ [(C_9 + C'_9) - (C_{10} + C'_{10})]\mathcal{F}_\parallel(q^2) + \frac{2m_b M_B}{q^2} [(C_7 + C'_7)\mathcal{F}_\parallel^T(q^2) - 16\pi^2 \frac{M_B}{m_b} \mathcal{H}_\parallel(q^2)] \right\},$$

where m_b and M_B are the masses of the b -quark and B^0 meson, respectively. This analysis fits data to directly extract the Wilson coefficients $C_{9,10}^{(\prime)}$ and the local and non-local form factors. The $C_7^{(\prime)}$ Wilson coefficients describe photon transitions and are fixed to their SM values^{18,19}.

The local form factors are constrained to determinations from lattice QCD²⁰ and light cone sum rules (LCSR)²¹. The non-local form factors are parametrised by¹⁵

$$\mathcal{H}_\lambda(z) = \frac{1 - z z_{J/\psi}}{z - z_{J/\psi}} \frac{1 - z z_{\psi(2S)}}{z - z_{\psi(2S)}} \hat{\mathcal{H}}_\lambda(z), \quad \hat{\mathcal{H}}_\lambda(z) = \phi_\lambda^{-1}(z) \sum_k a_{\lambda,k} z^k.$$

The variable z is a mapping of q^2 defined by

$$q^2 \mapsto z(q^2) \equiv \frac{\sqrt{t_+ - q^2} - \sqrt{t_+ - t_0}}{\sqrt{t_+ - q^2} + \sqrt{t_+ - t_0}},$$

where $t_+ = 4M_D$, with M_D being the D^0 mass, and t_0 chosen such that $z(q^2 = t_0) = 0$. The non-local form factors are thus an expansion in powers of the variable z . Measurements of $B^0 \rightarrow K^{*0}J/\psi$ and $B^0 \rightarrow K^{*0}\psi(2S)$ ^{22,23,24,25,26} are used to constrain the non-local functions at the poles. They have also been calculated with LCSR in the region $q^2 < 0 \text{ GeV}^2$ ²⁷, which may be used to add further constraints in the fit.

The data analysed are those collected by LHCb in Run 1 at $\sqrt{s} = 7, 8 \text{ TeV}$ and 2016 at $\sqrt{s} = 13 \text{ TeV}$, corresponding to an integrated luminosity of 4.7 fb^{-1} . This is the same data set as for the previous LHCb publication for $B^0 \rightarrow K^{*0}\mu^+\mu^-$ ⁶. At very low q^2 the data are dominated by decays with intermediate light resonances. At high q^2 $c\bar{c}$ resonances dominate.

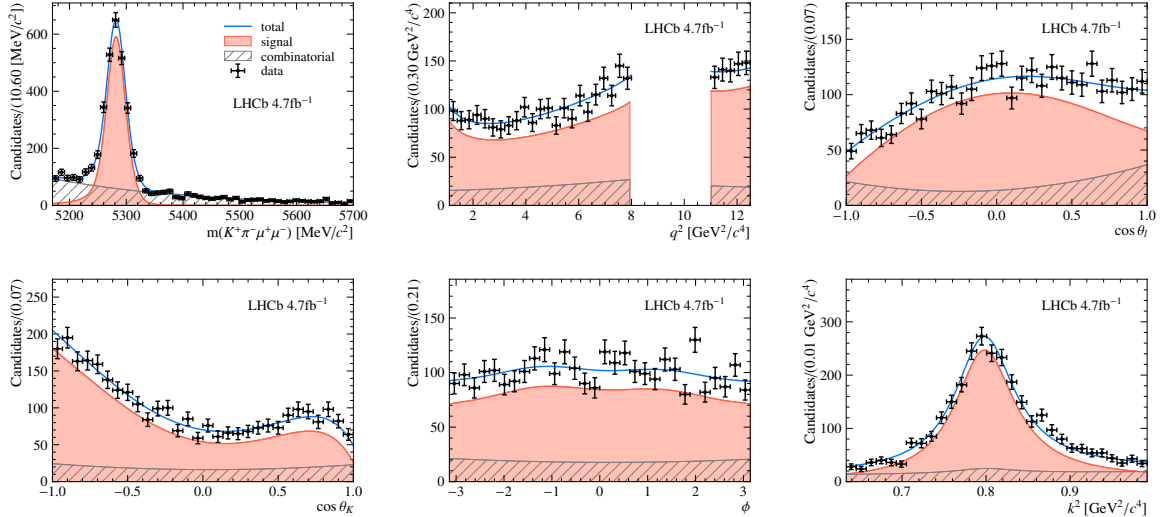


Figure 2: Fit projections.

Therefore a region in q^2 is selected below the J/ψ resonance, $1.1 < q^2 < 8.0 \text{ GeV}^2$ and between the J/ψ and $\psi(2S)$ resonances $11.0 < q^2 < 12.5 \text{ GeV}^2$. In this analysis the K^{*0} is reconstructed from $K^{*0} \rightarrow K^+\pi^-$.

The invariant mass of all the final state particles, $m(K^+\pi^-\mu^+\mu^-)$, is included in the fit to separate signal from backgrounds consisting of random combinations of tracks. The invariant mass of the $K^-\pi^+$ pair is also in the fit to separate out the contribution of the S-wave $B^0 \rightarrow K^+\pi^-\mu^+\mu^-$ decay. In total there are therefore six variables in the fit: $m(K^+\pi^-\mu^+\mu^-)$, $m(K^+\pi^-)$, $\cos\theta_\ell$, $\cos\theta_K$, ϕ and q^2 . The warping of the angular distributions due to the detector acceptance, track reconstruction and selection are modelled with large simulation samples and its effect is included in the fit following the procedure in the previous LHCb analysis⁶. The fit is carried out twice; once with the LCSR constraints for the non-local form factors at $q^2 < 0 \text{ GeV}^2$ and once without.

3 Results

The projections of the data with the fit result overlaid are shown in Fig. 2. The fit projections show no discernible change when fitting with or without the negative q^2 constraints.

The fitted local form-factors are shown in Fig. 3. The two fits are consistent with each other and broadly in agreement with the theory prediction. However it is noticeable in the ratios of form factors that the data prefers to pull down the values, compared to the predictions.

The fitted non-local form-factors are shown in Fig. 4. In general the agreement between the fits with or without the $q^2 < 0 \text{ GeV}^2$ predictions is good. The exception is in the imaginary part $\text{Im}(\mathcal{H}_\parallel)$ where the predictions provide a very tight constraint, whereas the data prefers to pull up the form-factors.

The one dimensional profiles of two of the Wilson coefficients of interest, C_9 and C_{10} , are shown in Fig. 5. The minima of the profiles are consistent with the fit is performed with or without the negative q^2 constraint. The result is that even with a contribution from non local effects the data prefers a value of the Wilson coefficient C_9 that is away from the SM prediction. When considering all four Wilson coefficients together the best fit point is found to be $1.3(1.4) \sigma$ from the SM when fitting without (with) the negative q^2 predictions.

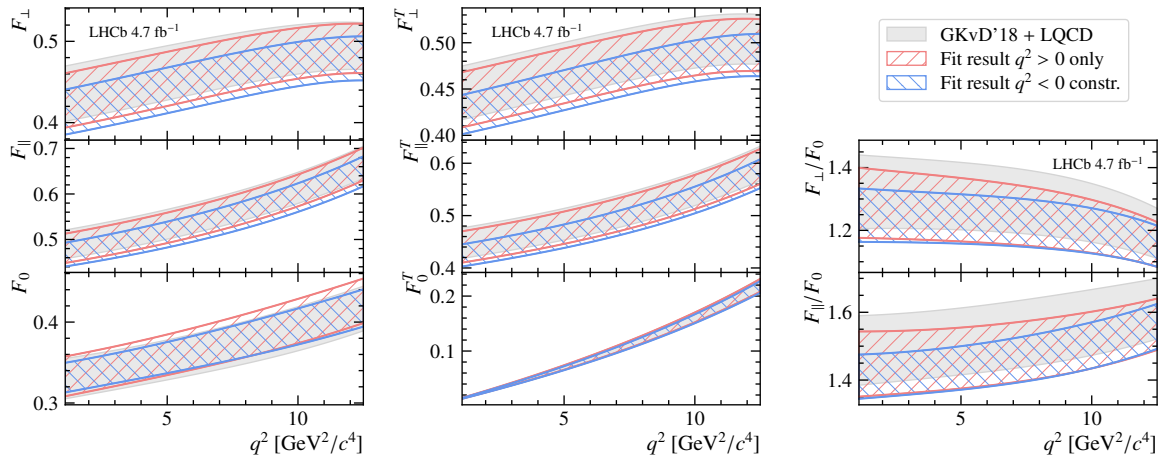


Figure 6: Absolute values

q^2 label

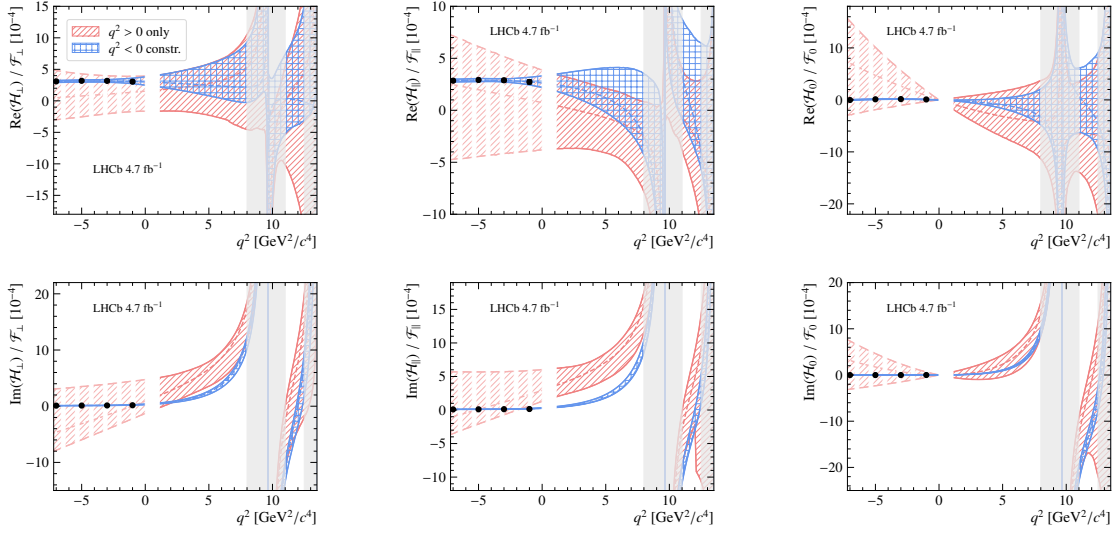


Figure 6: Real and imaginary parts

q^2 label

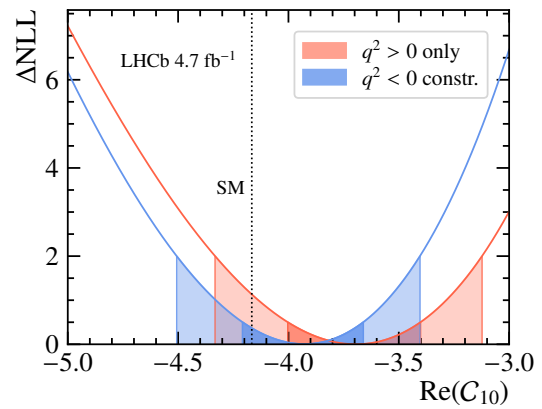
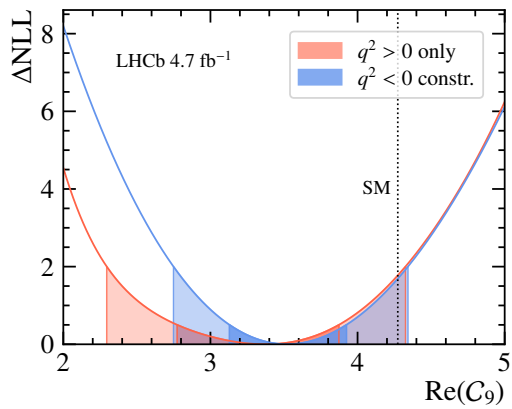


Figure 7: C_9

Figure 7: C_{10}

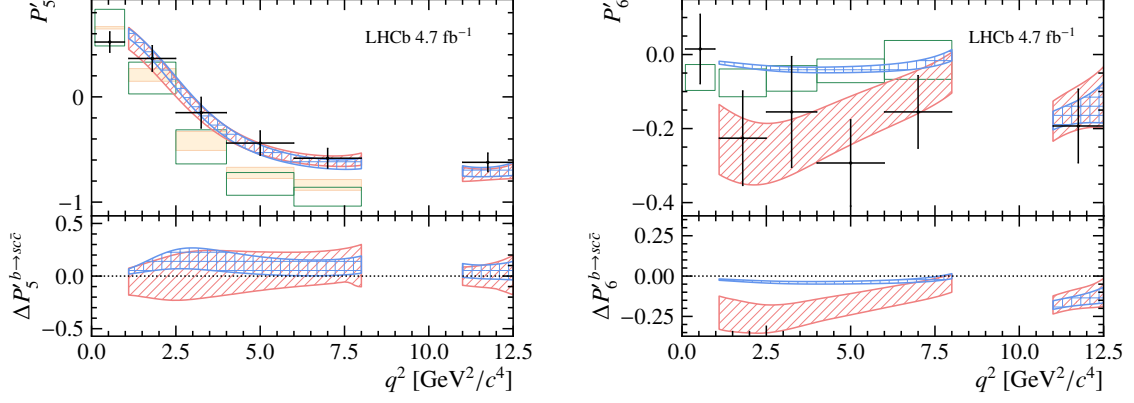


FIG. 6. Amplitude fits for P'_5 (left) and P'_6 (right). The top panel shows the fit with data points (black crosses) and shaded regions (green and blue) representing different fit components. The bottom panel shows the difference between the fit and the non-local contribution, $\Delta P'_i$, with shaded regions in red and blue. The text "LHCb 4.7 fb⁻¹" is present in the top right of each plot.

3.1 Comparison with binned results

The binned angular observables may be calculated from the fitted amplitudes to provide a direct comparison with the previous LHCb measurement ⁶. In addition, the non-local part of the amplitudes may be set to 0 in this calculation to provide an estimate of the non-local contribution to the measured binned observables. In general the agreement with the published binned analysis is good for the fits with or without the negative q^2 predictions. An example is P'_5 , shown in the left of Fig. 6. The exception is P'_6 (or S_7 for the non-optimised observables), shown in the right of Fig. 6. This observable is constructed from the imaginary parts of the amplitudes,

$$S_7 \sim \text{Im}(\mathcal{A}_0^L \mathcal{A}_{||}^{L*} - \mathcal{A}_0^R \mathcal{A}_{||}^{R*}).$$

Consequently the pull of the $q^2 < 0 \text{ GeV}^2$ predictions on the imaginary part of the non-local form factors produces a significant shift towards 0 when including them in the fit.

4 Conclusions

For the first time an amplitude fit of $B^0 \rightarrow K^{*0} \mu^+ \mu^-$ has been carried, unbinned in the q^2 variable. The resulting information is complementary to the previously published analyses. The fit has explicitly allowed for a contribution of long-distance $c\bar{c}$ amplitudes to try and disentangle the effects from long-distance and short-distance physics. It is found that even allowing for a long-distance contribution the data prefers the Wilson coefficient C_9 to be away from the Standard Model.

The LHCb collaboration still has much data in hand that is in the process of being analysed. In particular the binned analysis of $B^0 \rightarrow K^{*0} \mu^+ \mu^-$ using the full Run 1 and Run 2 data sets is awaited ²⁸. Furthermore, there is a second unbinned analysis using the full Run 1 and Run 2 data set that has recently been made public. This new analysis also tried to make an estimate of the non-local contributions by using a model of all of the $c\bar{c}$ resonances ^{29,30,31}. In addition there is a possibility of making a model-independent determination of the amplitudes of the decay that is continuous in q^2 ³².

The LHCb detector has recently started taking data for Run 3. The goal is to collect 7 fb^{-1} in 2024 at $\sqrt{s} = 13.6 \text{ TeV}$ which would represent an equivalent amount of data as that collected in Run 1 and Run 2. A similar harvest is envisaged for 2025 before the next long shutdown of the LHC. This Run 3 dataset will therefore provide a significant increase in precision for the study of these FCNC decay modes.

References

1. LHCb collaboration, *Phys. Rev. Lett.* **127**, 2021 (151801)
2. LHCb collaboration, *Phys. Rev. Lett.* **131**, 2023 (151801)
3. LHCb collaboration, *JHEP* **06**, 2014 (133)
4. LHCb collaboration, *Phys. Rev. Lett.* **131**, 2023 (051803)
5. LHCb collaboration, *Phys. Rev. D* **108**, 2023 (032002)
6. LHCb collaboration, *Phys. Rev. Lett.* **125**, 2020 (011802)
7. LHCb collaboration, *Phys. Rev. Lett.* **126**, 2021 (161802)
8. A. Khodjamirian *et al*, *JHEP* **89**, 2010 (89)
9. S. Descotes-Genon *et al*, *JHEP* **12**, 2014 (125)
10. G. Buchalla *et al*, *Rev. Mod. Phys.* **68**, 1996 (1125)
11. M. Algueró *et al*, *Eur. Phys. J. C* **83**, 2023 (648)
12. A. Greljo *et al*, *JHEP* **05**, 2023 (87)
13. M. Ciuchini *et al*, *Phys. Rev. D* **107**, 2023 (055036)
14. L. Geng *et al*, *Phys. Rev. D* **104**, 2021 (035029)
15. N. Gubernari *et al*, *JHEP* **09**, 2022 (133)
16. LHCb collaboration, *Phys. Rev. D* **109**, 2024 (052009)
17. LHCb collaboration, *Phys. Rev. Lett.* **132**, 2024 (131801)
18. C. Bobeth *et al*, *Nucl. Phys. B* **574**, 2000 (291)
19. M. Gorbahn and U. Haisch, *Nucl. Phys. B* **713**, 2005 (291)
20. R. Horgan *et al*, *PoS LATTICE 2014*, 2015 (372)
21. N. Gubernari *et al*, *JHEP* **01**, 2019 (150)
22. Belle collaboration, *Phys. Rev. D* **90**, 2014 (11)
23. BABAR collaboration, *Phys. Rev. D* **76**, 2007 (03)
24. Belle collaboration, *Phys. Rev. D* **88**, 2013 (07)
25. LHCb collaboration, *Phys. Rev. D* **88**, 2013 (05)
26. LHCb collaboration, *Eur. Phys. J. C* **72**, 2012 (8)
27. N. Gubernari *et al*, *JHEP* **02**, 2021 (88)
28. M. Algueró *et al*, *JHEP* **12**, 2021 (85)
29. T. Blake *et al*, *Eur. Phys. J. C* **78**, 2018 (6)
30. C. Cornella *et al*, *Eur. Phys. J. C* **80**, 2020 (12)
31. LHCb collaboration, LHCb-PAPER-2024-011
32. U. Egede *et al*, *JHEP* **84**, 2015 (6)